

Target Localization Techniques and Tools for MIMO Radar

Hana Godrich[°], Alexander M. Haimovich[°], and Rick S. Blum[†]

[°]New Jersey Institute of Technology, Newark, NJ 07102

[†]Lehigh University, Bethlehem, PA 18015-3084

[°][hg44,haimovich]@njit.edu, [†]rblum@eecs.lehigh.edu

Abstract

This paper presents a comparative study of target localization techniques for multiple-input multiple-output (MIMO) radar systems with widely spread elements with either non-coherent or coherent processing. The performance of localization techniques utilizing both processing techniques is evaluated based on a closed-form solution developed for the best linear unbiased estimator (BLUE). This estimator provides insight into the relation between the radar locations, target location, and localization accuracy through the use of the geometric dilution of precision (GDOP) metrics. The best achievable accuracy for the coherent case is obtained and a comparative study to the non-coherent case is provided. MIMO radar systems with coherent processing are shown to benefit from a coherency gain, compared with the case of non-coherent processing. This gain is proportional to the ratio of the signal carrier frequency to the effective bandwidth (typically of the order of hundreds). The footprint of multiple sensors provides a MIMO gain for both processing techniques. This MIMO gain is proportional to the product of the number of transmitting and receiving sensors. Further analysis of the later gain is made possible by the use of the GDOP contour maps that offer a clear understanding of the achievable accuracy at various target locations.

Index Terms

MIMO radar, spatial processing, adaptive array.

I. INTRODUCTION

MIMO radars are sensing systems that employ multiple transmit waveforms and have the ability to jointly process signals received at multiple receive antennas. Research in MIMO radar is rapidly expanding [1]-[16]. Elements of MIMO radar have the ability to transmit diverse waveforms ranging from independent to fully correlated [5]. MIMO radar may be configured with its antennas colocated or widely distributed over an area. MIMO radar with colocated antennas makes use of waveform diversity [4], while MIMO radar with distributed antenna takes advantage of the spatial diversity supported by the system configuration [1]. As each configuration and model has its strengths and

A. M. Haimovich work was supported by the U.S. Air Force Office of Scientific Research, Agreement FA9550-06-1-0026. R. S. Blum work was supported by the Air Force Research Laboratory under agreement No. FA9550-06-1-0041

challenges, it is already apparent that each configuration has the potential to make important contributions to the radar field. In [6] it is observed that MIMO radar has more degrees of freedom than systems with a single transmit antenna. These additional degrees of freedom support flexible time-energy management modes [7], lead to improved angular resolution [8],[9], and improve parameter identifiability [10]. With widely separated antennas, MIMO radar has the ability to improve radar performance by exploiting radar cross section (RCS) diversity [11], handle slow moving targets by exploiting Doppler estimates from multiple directions [12], and support high accuracy target localization [14]-[16].

As the potential for localization performance enhancement is evident from the ambiguity function [14], the lower bound on the attainable accuracy is set by developing the Cramer-Rao lower bound (CRLB) [17],[18]. The CRLB for the MIMO radar case is derived in [16], yielding the best achievable accuracy with coherent processing. In [16], it is shown that the CRLB reveals a coherency gain, proportional to the ratio between the signal carrier frequency and the signal effective bandwidth. In this paper, we review methods for target localization estimation in MIMO radar systems with coherent and non-coherent processing based on the best linear unbiased estimator (BLUE). The closed form solution of this estimator affords insight into the relation between sensors locations, target location, and localization accuracy. The BLUE mean squared error (MSE) is used to present a comparative view of the coherent vs. non-coherent MIMO radar systems localization accuracy. For non-coherent processing, it is necessary to synchronize the radars at baseband; for coherent processing, the radars need to be synchronized at RF. Note that our coherent/non-coherent terminology is limited to the processing for localization. Thus, a transmitted signal may have in-phase and quadrature components, yet the localization processing is non-coherent if it utilizes only information in the signal envelope. To establish a more comprehensive expression of these relations, a metric widely used in Global Positioning Systems (GPS) for mapping estimation precision and known as geometric dilution of precision (GDOP) is applied.

The paper is organized as follows: the system signal model is introduced in Section II. In Section III the BLUE target localization estimator is derived. The BLUE is developed for non-coherent processing in Section III-A and coherent processing in Section III-B to support a comparative study presented by the GDOP metric in Section IV. Finally, Section V concludes the paper.

II. SYSTEM MODEL

The MIMO radar scheme is based on a system with M transmitting radars and N receiving radars, widely distributed over a given geographical area. The transmitting and receiving radars are located in a two dimensional plane (x, y) . The M transmitters are arbitrarily located at coordinates $T_k = (x_{tk}, y_{tk})$, $k = 1, \dots, M$, and the N receivers are similarly arbitrarily located at coordinates $R_\ell = (x_{r\ell}, y_{r\ell})$, $\ell = 1, \dots, N$. A set of orthogonal waveforms is transmitted, with the lowpass equivalent $s_k(t)$, $k = 1, \dots, M$. The power of the transmitted waveforms is normalized such that the aggregate power transmitted by the sensors is constant, irrespective of the number of transmit sensors. To simplify the notation, the signal power term is embedded in the noise variance term such that the signal-to-noise ratio (SNR) at the transmitter, denoted SNR_t , and defined as the transmitted power by a sensor

divided by the noise power at a receiving sensor, is set at a desired level. Let all transmitted waveforms be narrowband signals with individual effective bandwidth β_k defined as $\beta_k^2 = \left[\left(\int_{W_k} f^2 |S_k(f)|^2 df \right) / \left(\int_{W_k} |S_k(f)|^2 df \right) \right]$, where the integration is over the range of frequencies with non-zero signal content W_k [19]. We further define the averaged effective bandwidth or rms bandwidth as $\beta^2 = \frac{1}{M} \sum_{k=1}^M \beta_k^2$ and the normalized bandwidth terms as $\beta_{R_k} = \beta_k / \beta$. The signals are narrowband in the sense that for a carrier frequency of f_c , the narrowband signal assumption implies $\beta_k^2 / f_c^2 \ll 1$ and $\beta^2 / f_c^2 \ll 1$. The target model follows the one developed in [16], generalizing the complex target model in [19] to a near-field scenario and distributed sensors. In [16] it is shown that a complex target located at $X = (x, y)$ may be equivalently defined as a point scatterer with complex amplitude ζ and time delays $\tau_{\ell k}(X)$. For simplicity, the following notation is used: $\tau_{\ell k} = \tau_{\ell k}(X)$.

It follows that the received signal model is then defined by:

$$r_\ell(t) = \sum_{k=1}^M \zeta \exp(-j2\pi f_c \tau_{\ell k}) s_k(t - \tau_{\ell k}) + w_\ell(t). \quad (1)$$

where $w_\ell(t)$ is a circularly symmetric, zero-mean, complex Gaussian noise, spatially and temporally white with autocorrelation function $\sigma_w^2 \delta(\tau)$. We define the vector of received signals as $\mathbf{r} = [r_1, r_2, \dots, r_N]^T$ for later use. Define the unknown target location $X = (x, y)$, unknown time delays $\tau_{\ell k}$, and unknown target complex amplitude $\zeta = \zeta^R + j\zeta^I$, where the notation specifies the real and imaginary components of ζ .

The radar system's goal is to estimate the target location $X = (x, y)$. The target location can be estimated directly, for example by formulating the maximum likelihood estimate (MLE) associated with (1). Alternatively, an indirect method is to estimate first the time delays $\tau_{\ell k}$. Subsequently, the target location can be computed from the solution to a set of equations of the form:

$$\tau_{\ell k} = \frac{1}{c} \left[\sqrt{(x_{tk} - x)^2 + (y_{tk} - y)^2} + \sqrt{(x_{r\ell} - x)^2 + (y_{r\ell} - y)^2} \right]. \quad (2)$$

We refer to the processing for estimating the target location as *non-coherent* or *coherent*. The received signal introduced in (1) is adequate for the coherent case, where the transmitting and receiving radars are assumed to be both time and phase synchronized. As such, the time delays information, $\tau_{\ell k}$, embedded in the phase terms may be exploited in the estimation process by matching both amplitude and phase at the receiver end. In contrast, non-coherent processing estimates the time delays $\tau_{\ell k}$ from variations in the envelope of the transmitted signals $s_k(t)$. A common time reference is required for all the sensors in the system. In this case, the transmitting radars are not phase synchronized and therefore the received signal model is of the form:

$$r_\ell(t) = \sum_{k=1}^M \alpha_{\ell k} s_k(t - \tau_{\ell k}) + w_\ell(t), \quad (3)$$

where the complex amplitude terms $\alpha_{\ell k}$ integrate the effect of the phase offsets between the transmitting and receiving sources and the target impact on the phase and amplitude of the transmitted signals. These elements are treated as unknown complex amplitudes, where $\alpha_{\ell k} = \alpha_{\ell k}^R + j\alpha_{\ell k}^I$. We define the following vector notations $\boldsymbol{\alpha} = [\alpha_{11}, \alpha_{12}, \dots, \alpha_{\ell k}, \dots, \alpha_{MN}]^T$.

III. METHODS FOR TARGET LOCALIZATION

The BLUE provides a closed form estimator and therefore enables the evaluation of the localization performance of the MIMO radar scheme. To formulate the BLUE, it is necessary to have an observation model in which observations change linearly with the target location coordinates. That is because it is inherent to the BLUE that the estimate is *linear*. To this end, we formulate a model in which the time delays are “observable.” Let the observed time delay associated with a transmitter-receiver pair be $\mu_{\ell k}$, then

$$\mu_{\ell k} = \tau_{\ell k} + \epsilon_{\ell k}, \quad \forall k = 1, \dots, M, l = 1, \dots, N, \quad (4)$$

where $\epsilon_{\ell k}$ is the “observation noise.” In practice, the time delays are not directly observable. Rather, they are estimated, for example by maximum likelihood, from the received signals. Then, the term $\epsilon_{\ell k}$ is the time delay estimation error. Our BLUE estimation problem of the target location should not be confused with the estimation of the time delays. The estimation of the time delays is just a preparatory step in setting up the “observations” of the BLUE model. Once, the observation model has been set up, it is necessary to ensure that the model between the time delays and target location is linear. Setting the origin of the coordinate system at some nominal estimate of the target location $X_c = (x_c, y_c)$, and preserving only linear terms of the Taylor expansion of expressions such as in (2), we can express the time delays as linear functions of x and y ,

$$\tau_{\ell k} \approx -\frac{x}{c} (\cos \phi_k + \cos \varphi_\ell) - \frac{y}{c} (\sin \phi_k + \sin \varphi_\ell), \quad (5)$$

where the angles ϕ_k and φ_ℓ are the bearings that the transmitting sensor k and receiving sensor ℓ , respectively, subtend with the reference axis (with the origin at the nominal estimate of the target location). The vertex of the angles is an arbitrary point in the neighborhood of the true target location.

Utilizing definitions:

$$\begin{aligned} a_{tx_k} &= \cos \phi_k; & b_{tx_k} &= \sin \phi_k; & k &= 1, \dots, M, \\ a_{rx_\ell} &= \cos \varphi_\ell; & b_{rx_\ell} &= \sin \varphi_\ell; & \ell &= 1, \dots, N, \\ \phi_k &= \tan^{-1} \left(\frac{y_c - y_{tk}}{x_c - x_{tk}} \right); & \varphi_\ell &= \tan^{-1} \left(\frac{y_c - y_{r\ell}}{x_c - x_{r\ell}} \right), \end{aligned} \quad (6)$$

we can express the linear model in the following simplified form:

$$\tau_{\ell k} = -\frac{x}{c} (a_{tx_k} + a_{rx_\ell}) - \frac{y}{c} (b_{tx_k} + b_{rx_\ell}). \quad (7)$$

We postulate the following linear model between the observable time delays $\boldsymbol{\mu} = [\mu_{11}, \mu_{12}, \dots, \mu_{NM}]^T$ and the vector of unknown parameters $\boldsymbol{\theta}$:

$$\boldsymbol{\mu} = \mathbf{D}\boldsymbol{\theta} + \boldsymbol{\epsilon}, \quad (8)$$

where the matrix \mathbf{D} defined the linear relation between $\boldsymbol{\tau}$ and the vector of unknowns $\boldsymbol{\theta}$. The vector $\boldsymbol{\epsilon} = [\epsilon_{11}, \epsilon_{12}, \dots, \epsilon_{NM}]^T$ is the $MN \times 1$ measurement noise vector. According to (8), the BLUE's "observations" are in the form of time delays. So an intermediate step of time delay estimation is implied.

For the linear and Gaussian model in (8), the BLUE is computed from the Gauss-Markov theorem [17] that states the BLUE of the unknown vector $\boldsymbol{\theta}$ is given by the expression:

$$\hat{\boldsymbol{\theta}}_{BLUE} = (\mathbf{D}^T \mathbf{C}_\epsilon^{-1} \mathbf{D})^{-1} \mathbf{D}^T \mathbf{C}_\epsilon^{-1} \boldsymbol{\mu}. \quad (9)$$

where \mathbf{C}_ϵ is the covariance matrix characterizing the "noise" terms $\epsilon_{\ell k}$.

The theorem also determines the error covariance matrix for the estimator $\hat{\boldsymbol{\theta}}_{BLUE}$ to be

$$\mathbf{C}_{BLUE} = (\mathbf{D}^T \mathbf{C}_\epsilon^{-1} \mathbf{D})^{-1}. \quad (10)$$

From this point onward, we develop the BLUE for the case of non-coherent and coherent processing, separately.

A. BLUE for Non-coherent Processing

We recall that in the section on the signal model, we defined the complex amplitude $\alpha_{\ell k}$ associated with the path transmitter $k \rightarrow$ target \rightarrow receiver ℓ in the received signal model given in (3). In the non-coherent case, the complex amplitude is a nuisance parameter in estimating the target location x, y . There is no common phase reference among the sensors and phase information is not exploited in the estimation process. **Consequently, the time observation, evaluated using non-coherent processing, are not affected by phase/time bias.** In this case, the vector of unknown parameters is defined as $\boldsymbol{\theta}_{nc} = [x, y]^T$ and the the time measurements are modeled as:

$$\mu_{nc\ell k} \approx -\frac{1}{c} [x (a_{tx_k} + a_{rx_\ell}) + y (b_{tx_k} + b_{rx_\ell})] + \epsilon_{nc\ell k}. \quad (11)$$

The relation in (11) can be written as:

$$\boldsymbol{\mu}_{nc} = \mathbf{D}_{nc} \boldsymbol{\theta}_{nc} + \boldsymbol{\epsilon}_{nc}, \quad (12)$$

where the observable time delays $\boldsymbol{\mu}_{nc} = [\mu_{nc11}, \mu_{nc12}, \dots, \mu_{ncNM}]^T$ are derived incoherently by the MLE as follows:

$$\mu_{nc\ell k} = \arg \max_v \left| \int r_\ell(t) s_k^*(t-v) dt \right|, \quad (13)$$

where v is a dummy variable for the time delay. Matrix \mathbf{D}_{nc} is defined as:

$$\mathbf{D}_{nc} = -\frac{1}{c} \begin{bmatrix} a_{tx_1} + a_{rx_1} & b_{tx_1} + b_{rx_1} \\ \dots & \dots \\ a_{tx_M} + a_{rx_N} & b_{tx_M} + b_{rx_N} \end{bmatrix}_{NM \times 2}. \quad (14)$$

It is shown in Appendix I that the maximum likelihood time delay estimates $\mu_{nc\ell k}$ are unbiased observations, where the measurement errors $\boldsymbol{\epsilon}_{nc} = [\epsilon_{nc11}, \epsilon_{nc12}, \dots, \epsilon_{ncNM}]^T$ have Gaussian distribution with zero mean and an error covariance matrix of the form

$$\mathbf{C}_{\boldsymbol{\epsilon}_{nc}} = \frac{1}{8\pi^2} \text{diag} \left(\frac{1}{\beta_1^2 \text{SNR}_{11}}, \frac{1}{\beta_1^2 \text{SNR}_{12}}, \dots, \frac{1}{\beta_M^2 \text{SNR}_{MN}} \right)_{NM \times NM}. \quad (15)$$

with $\text{SNR}_{\ell k} = \frac{|\alpha_{lk}|^2}{\sigma_w^2}$.

Using the time error covariance matrix $\mathbf{C}_{\boldsymbol{\epsilon}_{nc}}$ in (15) and the linear transformation matrix \mathbf{D}_{nc} in (14) to compute the BLUE, given by (9), the following estimate for the target localization with non-coherent processing is obtained:

$$\begin{bmatrix} \hat{x} \\ \hat{y} \end{bmatrix} = \begin{bmatrix} \hat{\boldsymbol{\theta}}_{nc} \end{bmatrix} = -\frac{8\pi^2 \beta^2}{c} \mathbf{U}_{nc} \begin{bmatrix} \sum_{k=1}^M \sum_{\ell=1}^N \beta_{R_k}^2 \text{SNR}_{lk} (a_{tx_k} + a_{rx_\ell}) \mu_{nc\ell k} \\ \sum_{k=1}^M \sum_{\ell=1}^N \beta_{R_k}^2 \text{SNR}_{lk} (b_{tx_k} + b_{rx_\ell}) \mu_{nc\ell k} \end{bmatrix}, \quad (16)$$

where $\mu_{nc\ell k}$ are the time observations, and the matrix \mathbf{U}_{nc} is of the form:

$$\begin{aligned} \mathbf{U}_{nc} &= (\mathbf{D}_{nc}^T \mathbf{C}_{\boldsymbol{\epsilon}_{nc}}^{-1} \mathbf{D}_{nc})^{-1} \\ &= \frac{\eta_{nc}}{(g_{1nc} g_{2nc} - h_{nc}^2)} \begin{bmatrix} g_{1nc} & h_{nc} \\ h_{nc} & g_{2nc} \end{bmatrix}. \end{aligned} \quad (17)$$

and

$$\begin{aligned} \eta_{nc} &= \frac{c^2}{8\pi^2 \beta^2}, \\ g_{1nc} &= \sum_{k=1}^M \sum_{\ell=1}^N \text{SNR}_{lk} \beta_{R_k}^2 (b_{tx_k} + b_{rx_\ell})^2, \\ g_{2nc} &= \sum_{k=1}^M \sum_{\ell=1}^N \text{SNR}_{lk} \beta_{R_k}^2 (a_{tx_k} + a_{rx_\ell})^2, \\ h_{nc} &= -\sum_{k=1}^M \sum_{\ell=1}^N \text{SNR}_{lk} \beta_{R_k}^2 (a_{tx_k} + a_{rx_\ell}) (b_{tx_k} + b_{rx_\ell}). \end{aligned} \quad (18)$$

Using these results in (10) provides the MSE for the BLUE as follows:

$$\sigma_{x,nc}^2 = \eta_{nc} \left(\frac{g_{1nc}}{g_{1nc} g_{2nc} - h_{nc}^2} \right), \quad (19)$$

for the estimation of the x coordinate, and

$$\sigma_{y,nc}^2 = \eta_{nc} \left(\frac{g_{2nc}}{g_{1nc} g_{2nc} - h_{nc}^2} \right), \quad (20)$$

for the estimation of the y coordinate.

B. BLUE for Coherent Processing

In the coherent case, the transmitting and receiving radars are assumed to be both time and phase synchronized. By eliminating the phase offsets, the signal model in (1) applies, and the nuisance parameter role is left to the complex target amplitude $\zeta = \zeta^R + j\zeta^I = r_\zeta \exp(j\phi_\zeta)$. The complex parameter ζ results in a common unknown time delay nuisance parameter δ , modeled as

$$\mu_{c\ell k} \approx -\frac{1}{c} [x(a_{tx_k} + a_{rx_\ell}) + y(b_{tx_k} + b_{rx_\ell}) + \delta] + \epsilon_{c\ell k}. \quad (21)$$

In this case, the vectors of unknown parameters is defined as $\boldsymbol{\theta}_c = [x, y, \delta]^T$ and the relation in (21) may be written

as:

$$\boldsymbol{\mu}_c = \mathbf{D}_c \boldsymbol{\theta}_c + \boldsymbol{\epsilon}_c, \quad (22)$$

where the observable time delays $\boldsymbol{\mu}_c = [\mu_{c11}, \mu_{c12}, \dots, \mu_{cNM}]^T$ are derived coherently by the MLE as follows:

$$\mu_{c\ell k} = \arg \max_v \left| \exp(j2\pi f_c v) \int r_\ell(t) s_k^*(t-v) dt \right|, \quad (23)$$

where v is a dummy variable for the time delay. Matrix \mathbf{D}_c is defined as:

$$\mathbf{D}_c = -\frac{1}{c} \begin{bmatrix} a_{tx_1} + a_{rx_1} & b_{tx_1} + b_{rx_1} & 1 \\ \dots & \dots & \dots \\ a_{tx_M} + a_{rx_N} & b_{tx_M} + b_{rx_N} & 1 \end{bmatrix}_{NM \times 3}. \quad (24)$$

It is shown in Appendix II that the maximum likelihood time delay estimates $\mu_{c\ell k}$ are unbiased observations where the measurement errors $\boldsymbol{\epsilon}_c = [\epsilon_{c11}, \epsilon_{c12}, \dots, \epsilon_{cNM}]^T$ have Gaussian distribution with zero mean and an error covariance matrix of the form

$$\mathbf{C}_{\epsilon_c} = \frac{1}{8\pi^2 f_c^2 \text{SNR}_\zeta} \mathbf{I}_{NM \times NM}. \quad (25)$$

where $\text{SNR}_\zeta = \frac{|\zeta|^2}{\sigma_w^2}$.

Using the time error covariance matrix \mathbf{C}_{ϵ_c} in (25) and the linear transformation matrix \mathbf{D}_c in (24) to compute the BLUE, given in (9), the following estimate for the target localization is obtained with coherent processing:

$$\begin{bmatrix} \hat{x} \\ \hat{y} \end{bmatrix} = \begin{bmatrix} \hat{\boldsymbol{\theta}}_c \end{bmatrix}_{2 \times 1} = -\frac{8\pi^2 f_c^2 \text{SNR}_\zeta}{c} \mathbf{U}_c \begin{bmatrix} \sum_{k=1}^M \sum_{\ell=1}^N (a_{tx_k} + a_{rx_\ell}) \mu_{c\ell k} \\ \sum_{k=1}^M \sum_{\ell=1}^N (b_{tx_k} + b_{rx_\ell}) \mu_{c\ell k} \end{bmatrix}, \quad (26)$$

where $\mu_{c\ell k}$ are the time observations, and the matrix \mathbf{U}_c is of the form:

$$\mathbf{U}_c = \frac{\eta_c}{(g_{1c} g_{2c} - h_c^2)} \begin{bmatrix} g_{1c} & h_c \\ h_c & g_{2c} \end{bmatrix}.$$

where:

$$\begin{aligned}
\eta_c &= \frac{c^2}{8\pi^2 f_c^2 \text{SNR}_\zeta}, \\
g_{1c} &= \sum_{k=1}^M \sum_{\ell=1}^N (b_{tx_k} + b_{rx_\ell})^2 - \frac{1}{MN} \left(\sum_{k=1}^M \sum_{\ell=1}^N (b_{tx_k} + b_{rx_\ell}) \right)^2, \\
g_{2c} &= \sum_{k=1}^M \sum_{\ell=1}^N (a_{tx_k} + a_{rx_\ell})^2 - \frac{1}{MN} \left(\sum_{k=1}^M \sum_{\ell=1}^N (a_{tx_k} + a_{rx_\ell}) \right)^2, \\
h_c &= - \sum_{k=1}^M \sum_{\ell=1}^N (a_{tx_k} + a_{rx_\ell}) (b_{tx_k} + b_{rx_\ell}) \\
&\quad + \frac{1}{MN} \sum_{k=1}^M \sum_{\ell=1}^N (a_{tx_k} + a_{rx_\ell}) \sum_{k=1}^M \sum_{\ell=1}^N (b_{tx_k} + b_{rx_\ell}) ..
\end{aligned} \tag{27}$$

Using these results in (10) provides the MSE for the BLUE as follows:

$$\sigma_{x,c}^2 = \eta_c \left(\frac{g_{1c}}{g_{1c}g_{2c} - h_c^2} \right), \tag{28}$$

for the estimation of the x coordinate, and

$$\sigma_{y,c}^2 = \eta_c \left(\frac{g_{2c}}{g_{1c}g_{2c} - h_c^2} \right), \tag{29}$$

for the estimation of the y coordinate.

C. Discussion

The expressions for the BLUE MSEs for the target location estimates as given in (19), (20), (28) and (29) provide insight into the performance of non-coherent vs. coherent MIMO radars, as follows:

- The BLUE MSEs ratios:

$$\begin{aligned}
\frac{\sigma_{x,nc}^2}{\sigma_{x,c}^2} &= \frac{f_c^2}{\beta^2} \left(\frac{g_{1c}g_{2c} - h_c^2}{g_{1c}} \frac{g_{1nc}}{g_{1nc}g_{2nc} - h_{nc}^2} \right) \\
\frac{\sigma_{y,nc}^2}{\sigma_{y,c}^2} &= \frac{f_c^2}{\beta^2} \left(\frac{g_{1c}g_{2c} - h_c^2}{g_{2c}} \frac{g_{2nc}}{g_{1nc}g_{2nc} - h_{nc}^2} \right),
\end{aligned} \tag{30}$$

where we assume $\text{SNR}_{\ell k} = \text{SNR}_\zeta = \text{SNR}_o$, $\beta_{R_k}^2 \simeq 1$, demonstrates a coherency gain that offers an accuracy advantage of the order f_c/β . Designing the ratio f_c/β to be in the range 100-1000, leads to dramatic gains. Though, this performance gain comes with a price; coherent processing poses the challenge of dealing with the ambiguities stemming from the large separation between sensors and the need for phase synchronization [2].

- The MSEs terms are strongly reliant on the footprint of the radar system relative to the target location. This relation is incorporated into the terms $\frac{g_{1nc/c}}{g_{1nc/c}g_{2nc/c} - h_{nc/c}^2}$ and $\frac{g_{2nc/c}}{g_{1nc/c}g_{2nc/c} - h_{nc/c}^2}$. These terms incorporate gains inherent in the footprint of the MIMO radar system, defined herein as MIMO gains. However, the relations between the location dependent terms in (30) are not readily discerned, and further analysis is desirable.
- There is a performance trade-off between the MSE of the target location estimation computed for the x and y axes. A set of sensor locations that minimizes the MSE on the x coordinate, σ_x^2 , may result in a high MSE on the y coordinate, σ_y^2 . In order to truly determine the minimum achievable localization accuracy, the *overall*

accuracy needs to be optimized, i.e., optimize the MSE of the x and y coordinates jointly by optimizing $\sigma_{xy}^2 = (\sigma_x^2 + \sigma_y^2)$. In [16], it is shown, using the CRLB, that in the coherent case, the best overall accuracy is obtained when the transmitting and receiving radars are placed with uniform angular spacings of $2\pi/M$ and $2\pi/N$, respectively, around the target position, or any *superposition* of such sets. This applies to the BLUE MSE, since it asymptotically achieves the CRLB [17] for the case of Gaussian data. Under these conditions, the lowest overall BLUE MSE with coherent processing is given by $[\sigma_{xy,c}^2]_{c_opt_set} = \frac{c^2}{8\pi^2 f_c^2 \text{SNR}_o} \frac{2}{MN}$. In the non-coherent case, it can be easily shown that such a constellation of sensors will produce $[\sigma_{xy,nc}^2]_{c_opt_set} = \frac{c^2}{8\pi^2 \beta^2 \text{SNR}_o} \frac{2}{MN}$, although it is not necessarily the optimal value of $\sigma_{xy,nc}^2$.

Since the effect of the radars and the target positions on the obtainable accuracy cannot be intuitively identified from the terms of (30), a more suitable method to express these relations is employed in the next section. These evaluation tools incorporate the mapping of accuracy gain metric over a given geographical area, acting as a design and decision making mechanism for MIMO radar systems.

IV. GDOP METRIC

The GDOP metric is commonly used in GPS for mapping the attainable localization precision for a given layout of GPS satellites positions [21]- [23]. Here, we seek a metric that expresses the effect of the positions of the transmitting and receiving elements of the MIMO radar on the relationship between the time delay estimation errors and the localization errors. Plots of GDOP provide a clear view of high accuracy areas for a given set of radar locations. In non-exclusive GPS applications the term GDOP is sometimes replaced by the term PDOP (position dilution of precision) [24].

The GDOP metric is commonly defined as:

$$\text{GDOP} = \frac{1}{\sigma_R} \text{tr}(\text{cov}(X)) \quad (31)$$

where σ_R^2 is the range (delay) measurements error, defined by standard deviation of the time delays $c^2\sigma_\epsilon^2$. $\text{cov}(X)$, where $\text{cov}(\circ)$ stands for the covariance matrix. For the two dimensional case, where $X = (x, y)$, it is:

$$\text{GDOP} = \sqrt{\frac{\sigma_x^2 + \sigma_y^2}{c^2\sigma_\epsilon^2}}, \quad (32)$$

where σ_x^2 and σ_y^2 are the variances of localization on the x and y axis, respectively. We further define two one dimensional metrics: the horizontal x-axis DOP (HxDOP) and horizontal y-axis DOP (HyDOP), as:

$$\text{HxDOP} = \sqrt{\frac{\sigma_x^2}{c^2\sigma_\epsilon^2}}, \quad (33)$$

$$\text{HyDOP} = \sqrt{\frac{\sigma_y^2}{c^2\sigma_\epsilon^2}}. \quad (34)$$

We can use the BLUE MSEs given in (19), (20), (28) and (29), and the time delay variance in (15) and (25), to evaluate the GDOP metric for MIMO radar systems with non-coherent and coherent processing. The following GDOP expression is obtained for the non-coherent case:

$$\text{GDOP}_{B_{nc}} = \sqrt{\frac{g_{1_{nc}} + g_{2_{nc}}}{(g_{1_{nc}}g_{2_{nc}} - h_{nc}^2)}} \quad (35)$$

$$= \sqrt{\frac{c^2}{8\pi^2\beta^2\text{SNR}_o}}\sigma_{xy,nc}^2, \quad (36)$$

where we assume $\text{SNR}_{\ell k} = \text{SNR}_c = \text{SNR}_o$, $\beta_{R_k}^2 \simeq 1$ and therefore, $\sigma_{\epsilon_{nc}}^2 = \frac{1}{8\pi^2\beta^2\text{SNR}_o} = \frac{\eta_{nc}}{c^2}$.

For coherent processing we have:

$$\text{GDOP}_{B_c} = \sqrt{\frac{g_{1_c} + g_{2_c}}{(g_{1_c}g_{2_c} - h_c^2)}} \quad (37)$$

$$= \sqrt{\frac{c^2}{8\pi^2f_c^2\text{SNR}_o}}\sigma_{xy,c}^2, \quad (38)$$

where $\sigma_{\epsilon_c}^2 = \frac{1}{8\pi^2f_c^2\text{SNR}_o} = \frac{\eta_c}{c^2}$.

In the GDOP expressions in (35) and (37), the sensors' locations are embedded in the terms a_{tx_k} , a_{rx_ℓ} , b_{tx_k} and b_{rx_ℓ} as defined in (18) and (27). The GDOP reduces the combined effect of the locations to a single metric. In this case, the metric is a representation of the MIMO gain. Once we get the values mapped, the actual localization overall accuracy σ_{xy}^2 is easily derived by multiplying the GDOP value by $c\sigma_\epsilon$, and for either the x or y coordinates accuracy, by multiplying the HxDOP and HyDOP by $c\sigma_\epsilon$.

In Figures 1 and 2, contour plots of the GDOP values are presented for the case of non-coherent and coherent processing, respectively, with $M = N = 4$ radars positioned symmetrically on the $M + N$ vertices of a polygon centered at the origin. The radars are all transmitting orthogonal signals and perform time delay estimations. The GDOP value for a target located at the origin is the same in both plots. This value is consistent with the results indicated in the previous section, i.e., the minimal achievable overall MSE is equal to $[\sigma_{xy,c}^2]_{c_opt_set} = \frac{c^2}{8\pi^2f_c^2\text{SNR}_o} \frac{2}{MN} = c^2\sigma_\epsilon^2 \text{GDOP}_{B_{c_opt}}^2$ and, therefore, $\text{GDOP}_{B_{c_opt}} = \sqrt{\frac{2}{MN}}$. In Figure 2, The GDOP value for a target located at the origin follows the analytical result with $\text{GDOP}_{B_{c_opt}} = \sqrt{\frac{2}{16}} = 0.35355$. It is noticeable that while this value is minimal for coherent processing, this is not the case for non-coherent processing, where curves indicating GDOP values of 0.32 and 0.34 may be found in Figure 1. The distribution of the GDOP values has different characteristics for each case. In the coherent case, targets located inside the virtual $(N + M)$ -sided polygon formed by the sensors locations demonstrate lower GDOP values than targets located outside the footprint of the polygon. In particular, the best localization is obtained for a target at the center of the system. The increase in GDOP values from the center to the polygon perimeter is slow. Outside the footprint, the GDOP values increase rather rapidly (as manifested by the density of contours). In the non-coherent case, the lowest GDOP values are obtained at the perimeter of the virtual $(N + M)$ -sided polygon. The distribution of the GDOP value inside the

virtual polygon footprint is almost uniform. Outside the system footprint, a slow increase in the GDOP values is observed.

Contour maps of the HxDOP and HyDOP are presented in Figures 3 and 4, respectively. The radars are located in a similar manner to the one given in Figures 1 and 2. The trade-off between the accuracy gains achievable in either the x and y coordinates is demonstrated. In Figure 3, the curves with the lowest HxDOP values, ranging from $0.24 - 0.25$, are obtained in the upper and lower most part of the map. Similarly, in Figure 4, the lower HyDOP curves, within the same range, are obtained in the right and left most part of the map. With both metrics, a target located at the origin benefits from low HxDOP and HyDOP values (of the order 0.25). In the case when better accuracy is required on a single coordinate, the HxDOP and HyDOP maps may serve in the decision making.

In Figures 5 and 6 contours of $M = N = 4$ of non-symmetrically positioned radars are drawn for non-coherent and coherent processing. When the radars are not spread around the target there is a marked degradation in areas with good measurement accuracy with coherent processing, as demonstrated in Figure 6. These examples show that a symmetrical deployment of sensors around the target yields better GDOP values for coherent processing. Non-coherent processing (Figure 5) does not show significant degradation with asymmetric placement, though the distribution of lower GDOP curves is different compared with the one observed in Figure 1.

Plots of GDOP provide a clear view of high accuracy areas for a given set of radar locations. These plots could also serve as a tool for choosing favorable radar locations to cover a given target area.

V. CONCLUSIONS

The MIMO radar architecture with coherent processing exploits knowledge of the phase differences measured at the receive antennas to produce a high accuracy target location estimate. We showed that by exploiting the spatial dimension, MIMO radar with widely separated antennas may overcome bandwidth limitations and support high accuracy target localization. Coherent processing is shown to reduce the MSE values (standard deviation of the estimates) by a factor of f_c/β over the case when the observations are non-coherent. Nonetheless, both processing methods benefit from a MIMO gain directly proportional to the product of the number of transmitting and receiving radars. At the same time, this type of MIMO radar has the challenge of time and/or phase synchronizing multisite systems, and needs to deal with ambiguities stemming from the large separation between sensors. GDOP contours, mapping the relative performance accuracy for a given layout of radars over a given geographic area, were introduced. These plots offer a clear understanding of the collaboration effect of different sensor schemes on the resulting accuracy for both processing schemes.

APPENDIX I

DERIVATION OF (15)

For a set of received waveforms $r_\ell(t)$, $1 \leq \ell \leq N$, in (3), the time delay estimates $\mu_{nc} = [\mu_{nc_{11}}, \mu_{nc_{12}}, \dots, \mu_{nc_{MN}}]^T$ are determined by maximizing the following statistic:

$$\mu_{nc\ell k} = \arg \max_v \left| \int_T r_\ell(t) s_k^*(t-v) dt \right|. \quad (39)$$

Equivalently,

$$\left[\int_T \frac{d}{dv} [\alpha_{\ell k} s_k(t - \tau_{\ell k}) + w_\ell(t)] s_k^*(t-v) dt \right]_{v=\mu_{nc\ell k}} = 0. \quad (40)$$

The time delay estimates are expressed in (4). The properties of the noise $\epsilon_{\ell k}$ can be computed from (2), and (3). It is not difficult to show that the following relation holds:

$$\frac{dg_{nc}(v)}{dv} \Big|_{v=\mu_{nc\ell k}} + n_{nc\ell k} = 0, \quad (41)$$

where

$$g_{nc}(v) = \alpha_{\ell k} \int_T s_k(t - \tau_{\ell k}) s_k^*(t-v) dt, \quad (42)$$

and

$$n_{nc\ell k} = \int_T \frac{d}{dv} w_\ell(t) s_k^*(t-v) dt. \quad (43)$$

We wish to write (51) in the form of (4). With a few algebraic manipulations, including expanding $g_{nc}(v)$ in a Taylor series around $\tau_{\ell k}$, and neglecting terms $o\left[(\tau_{\ell k} - \mu_{nc\ell k})^3\right]$, it can be shown that

$$\hat{\tau}_{\ell k} = \tau_{\ell k} + \frac{n_{nc\ell k} \alpha_{\ell k}}{4\pi^2 \beta_k^2 |\alpha_{\ell k}|^2}. \quad (44)$$

Comparing this with (4), we have for the error term

$$\epsilon_{nc\ell k} \simeq \frac{n_{nc\ell k} \alpha_{\ell k}}{4\pi^2 \beta_k^2 |\alpha_{\ell k}|^2}. \quad (45)$$

To find the first and second order statistics of $\epsilon_{nc\ell k}$, we need the statistical characterization of $n_{\ell k}$. As previously stated, we assume the receiver noise $w_\ell(t)$ is a Gaussian random process with zero mean and autocorrelation function $\sigma_w^2 \delta(\tau)$. Since $n_{\ell k}$ is a linear transformation of the process $w_\ell(t)$, since the mean $w_\ell(t)$ is zero, $E[n_{\ell k}] = 0$. Similarly, it can be shown that

$$E[n_{nc\ell k} n_{ncnm}] = \begin{cases} 0 & \forall \ell k \neq nm \\ 2\pi^2 \sigma_w^2 \beta_k^2 & \forall \ell k = nm \end{cases}. \quad (46)$$

Using these results, we finally get

$$\begin{aligned} E[\epsilon_{nc\ell k} \epsilon_{ncnm}] &= \frac{E[n_{nc\ell k} n_{ncnm}]}{16\pi^4 \beta_k^4 |\alpha_{\ell k}|^2} \\ &= \begin{cases} 0 & \forall \ell k \neq nm \\ \frac{1}{8\pi^2 \beta_k^2 (|\alpha_{\ell k}|^2 / \sigma_w^2)} & \forall \ell k = nm \end{cases}, \end{aligned} \quad (47)$$

concluding that the covariance matrix of the terms $\epsilon_{nc\ell k}$ is given by:

$$\mathbf{C}_{\epsilon_{nc}} = \frac{1}{8\pi^2} \text{diag} \left(\frac{1}{\beta_1^2 \text{SNR}_{11}}, \frac{1}{\beta_1^2 \text{SNR}_{12}}, \dots, \frac{1}{\beta_M^2 \text{SNR}_{MN}} \right)_{MN \times MN}. \quad (48)$$

where $\text{SNR}_{\ell k} = \frac{|\alpha_{\ell k}|^2}{\sigma_w^2}$.

APPENDIX II
DERIVATION OF (25)

For a set of received waveforms $r_\ell(t)$, $1 \leq \ell \leq N$, in (1), the time delay estimates $\mu_c = [\mu_{c_{11}}, \mu_{c_{12}}, \dots, \mu_{c_{MN}}]^T$ are determined by maximizing the following statistic:

$$\mu_{c_{\ell k}} = \arg \max_v \left| \exp(j2\pi f_c v) \int_T r_\ell(t) s_k^*(t-v) dt \right|. \quad (49)$$

Equivalently,

$$\left[\int_T \frac{d}{dv} \zeta \exp(j2\pi f_c v) [\exp(-j2\pi f_c \tau_{\ell k}) s_k(t - \tau_{\ell k}) + w_\ell(t)] s_k^*(t-v) dt \right]_{v=\mu_{c_{\ell k}}} = 0. \quad (50)$$

The time delay estimates are expressed in (4). The properties of the noise $\epsilon_{c_{\ell k}}$ can be computed from (2), and (1). It is not difficult to show that the following relation holds:

$$\left. \frac{dg_c(v)}{dv} \right|_{v=\mu_{c_{\ell k}}} + n_{c_{\ell k}} = 0, \quad (51)$$

where

$$g_c(v) = \zeta \int_T \exp[j2\pi f_c (v - \tau_{\ell k})] s_k(t - \tau_{\ell k}) s_k^*(t-v) dt, \quad (52)$$

and

$$n_{c_{\ell k}} = \int_T \frac{d}{dv} w_\ell(t) s_k^*(t-v) \exp(j2\pi f_c v) dt. \quad (53)$$

We wish to write (51) in the form of (4). With a few algebraic manipulations, including expanding $g_c(v)$ in a Taylor series around $\tau_{\ell k}$, and neglecting terms $o[(\tau_{\ell k} - \mu_{c_{\ell k}})^3]$, it can be shown that

$$\mu_{c_{\ell k}} = \tau_{\ell k} + \frac{n_{c_{\ell k}} \zeta}{4\pi^2 f_c^2 \left(1 + \frac{\beta_k^2}{f_c^2}\right) |\zeta|^2}. \quad (54)$$

Comparing this with (4), and invoking the narrowband assumption $\beta_k^2/f_c^2 \ll 1$, we have for the error term

$$\epsilon_{c_{\ell k}} \simeq \frac{n_{c_{\ell k}} \zeta}{4\pi^2 \zeta f_c^2 |\zeta|^2}. \quad (55)$$

To find the first and second order statistics of $\epsilon_{c_{\ell k}}$, we need the statistical characterization of $n_{c_{\ell k}}$. As previously stated, we assume the receiver noise $w_\ell(t)$ is a Gaussian random process with zero mean and autocorrelation function $\sigma_w^2 \delta(\tau)$. Since $n_{c_{\ell k}}$ is a linear transformation of the process $w_\ell(t)$, since the mean $w_\ell(t)$ is zero, $E[n_{c_{\ell k}}] = 0$. Similarly, it can be shown that

$$E[n_{c_{\ell k}} n_{c_{nm}}] = \begin{cases} 0 & \forall \ell k \neq nm \\ 2\pi^2 \sigma_w^2 f_c^2 & \forall \ell k = nm \end{cases}. \quad (56)$$

Using these results, we finally get

$$\begin{aligned} E[\epsilon_{c_{\ell k}} \epsilon_{c_{nm}}] &= \frac{E[n_{c_{\ell k}} n_{c_{nm}}]}{16\pi^4 |\zeta|^2 f_c^4} \\ &= \begin{cases} 0 & \forall \ell k \neq nm \\ \frac{1}{8\pi^2 f_c^2 (|\zeta|^2 / \sigma_w^2)} & \forall \ell k = nm \end{cases}, \end{aligned} \quad (57)$$

concluding that the covariance matrix of the terms $\epsilon_{c\ell k}$ is given by:

$$\mathbf{C}_{\epsilon_c} = \frac{1}{8\pi^2 f_c^2 \text{SNR}_\zeta} \mathbf{I}_{MN \times MN}. \quad (58)$$

where $\text{SNR}_\zeta = \frac{|\zeta|^2}{\sigma_w^2}$.

REFERENCES

- [1] E. Fishler, A. M. Haimovich, R. S. Blum, L. Cimini, D. Chizhik, and R. Valenzuela, "MIMO radar: an idea whose time has come," in *Proc. of the 2004 IEEE Int. Conf. on Radar*, April 2004, pp. 71–78.
- [2] A. Haimovich, R. Blum, L. Cimini, , "MIMO Radar with Widely Separated antennas", *IEEE Signal Proc. Magazine*, January 2008.
- [3] H. Godrich, A.M Haimovich, and R.S. Blum, "Concepts And Applications Of MIMO Radar System With Widely Separated Antenna.," Book Chapter, in preparation, 2008.
- [4] J. Li, and P. Stoica, "MIMO Radar with Colocated antennas", *IEEE Signal Proc. Magazine*, September 2007, pp. 106–114.
- [5] D. R. Fuhrman, and G. San Antonio, "Transmit beam-forming for MIMO radar systems using partial signal correlation," in *Proc. of 38th ASILOMAR 2004 Conf. on Signals, Systems and Computers*, Nov. 2004, pp. 295–299.
- [6] D. W. Bliss, and K. W. Forsythe, "Multiple-input multiple-output (MIMO) radar and imaging: degrees of freedom and resolution," in *Proc. of 37th ASILOMAR 2003 Conf. on Signals, Systems and Computers*, Nov. 2003, pp. 54–59.
- [7] D. Rabideau, "Ubiquitous MIMO digital array radar," in *Proc. of 37th ASILOMAR 2003 Conf. on Signals, Systems and Computers*, Nov. 2003, pp. 1057–1064.
- [8] F. C. Robey, S. Coutts, D. Weikle, J. C. McHarg, and K. Cuomo, "MIMO radar theory and experimental results," in *Proc. of 37th ASILOMAR 2004 Conf. on Signals, Systems and Computers*, Nov. 2004, pp. 300–304.
- [9] I. Bekkerman and J. Tabrikian, "Target detection and localization using MIMO radars and sonars," *IEEE Trans. on Sig. Proc.*, vol. 54, pp. 3873–3883, Oct. 2006.
- [10] L. Xu, J. Li, and P. Stoica, "Adaptive techniques for MIMO radar," in *14th IEEE Workshop on Sensor Array and Multi-channel Processing*, Waltham, MA, July 2006.
- [11] E. Fishler, A. M. Haimovich, R. S. Blum, L. Cimini, D. Chizhik, and R. Valenzuela, "Spatial diversity in radars – models and detection performance," *IEEE Trans. on Sig. Proc.*, vol. 54, pp. 823–838, March 2006.
- [12] N. Lehmann, A. M. Haimovich, R. S. Blum, and L. Cimini, "MIMO – radar application to moving target detection in homogenous clutter," in *14th IEEE Workshop on Sensor Array and Multi-channel Processing*, Waltham, MA, July 2006.
- [13] A. S. Fletcher, and F. C. Robey, "Performance bounds for adaptive coherence of sparse array radar," in *Proc. of the 11th Conf. on Adaptive on Sensor Array and Multi-channel Processing*, March 2003.
- [14] N. Lehmann, A. M. Haimovich, R. S. Blum, and L. Cimini, "High resolution capabilities of MIMO radar," in *Proc. of 40th ASILOMAR 2006 Conf. on Signals, Systems and Computers*, Nov. 2006.
- [15] H. Godrich, A. M. Haimovich, and R. S. Blum, "Cramer Rao Bound on Target Localization Estimation in MIMO Radar Systems", in *Proc. of CISS Conf.*, March 2008.
- [16] H. Godrich, A. M. Haimovich, and R. S. Blum, "Target localization accuracy gain in MIMO radar based system," submitted to *IEEE Trans. on Information Theory*.
- [17] S. M. Kay, *Fundamentals of Statistical Signal Processing: Estimation Theory*, vol. 1, New Jersey: Parentice Hall PTR, 1st ed., 1993.
- [18] F. Gini and R. Reggiannini "The Modified Cramér-Rao Bound in Vector Parameter Estimation," *IEEE Trans. on Communications*, vol. 46, No. 1, pp. 52-60, Jan 1998.
- [19] M. Skolnik, *Introduction to Radar Systems*. New York: McGraw-Hill, 3rd, 2002.
- [20] N. Levanon, *Radar Principles*. New York: John Wiley and Sons Inc., 1st ed., 1988.
- [21] H. B. Lee, "A novel procedure for assessing the accuracy of the hyperbolic multilateration systems," *IEEE Trans. on Aerospace and Electronic Systems*, vol. 11, pp. 2–15, Jan. 1975.
- [22] N. Levanon, "Lowest GDOP in 2-D scenarios," *IEE Proc. –Radar, Sonar, Navig.*, vol. 147, pp. 149–155, June 2000.

- [23] R. Yarlagadda, I. Ali, N. Al-Dhahir, and J. Hershey, "GPS GDOP metric," *IEE Proc. –Radar, Sonar, Navig.*, vol. 147, No. 5, pp. 259-264, October 2000.
- [24] B. W. Parkinson and J. J. Spilker, *Global Positioning System: Theory and Applications*. AIAA, 1995.
- [25] S. Haykin, *Radar Array Processing*, Springer, 1993.

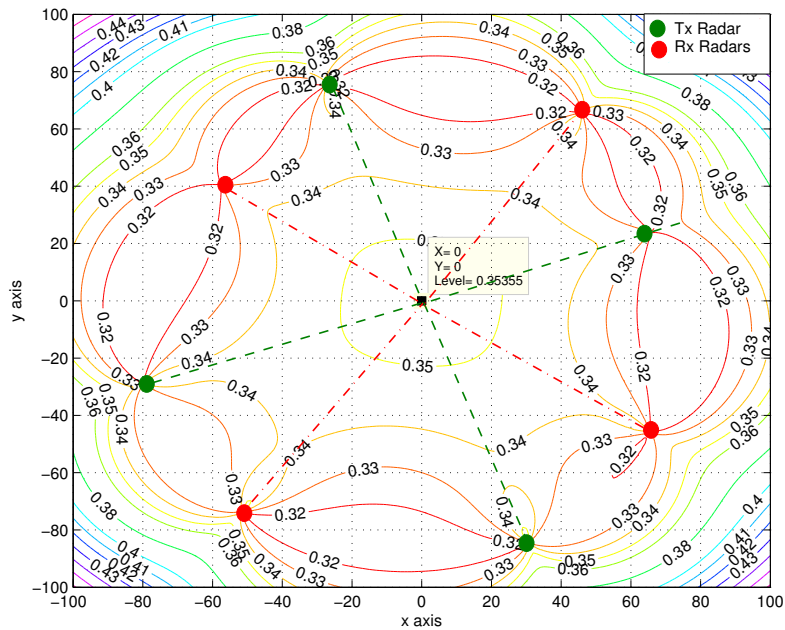


Figure 1: Non-coherent GDOP contours with $M=N=4$.

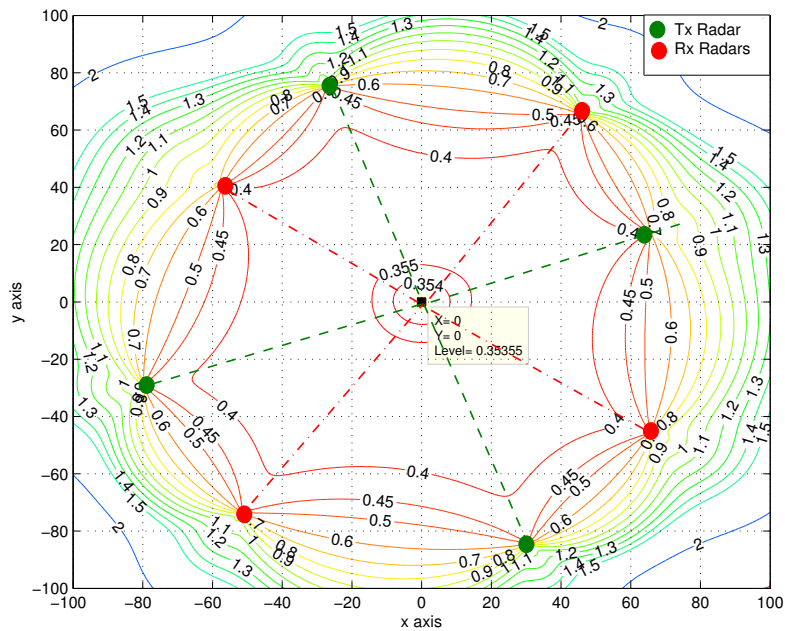


Figure 2: Coherent GDOP contours with $M=N=4$.

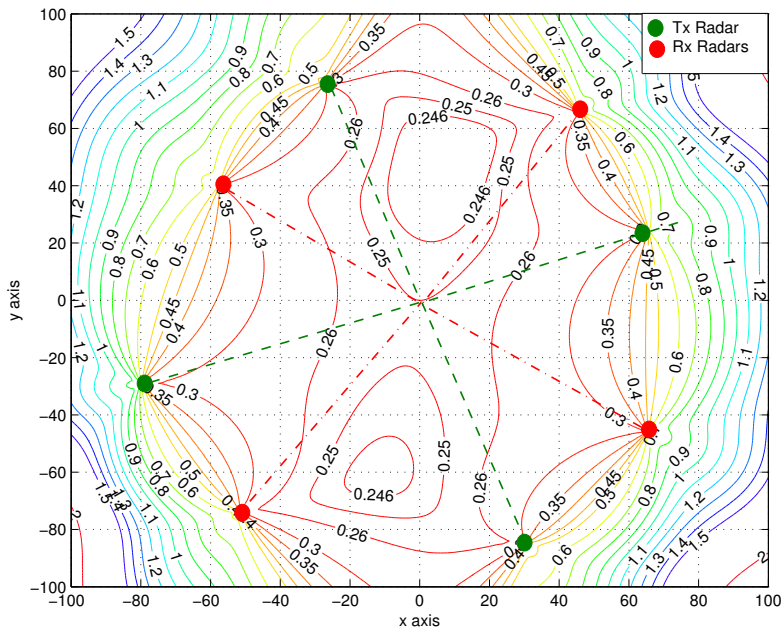


Figure 3: Coherent HxDOP contours with $M=N=4$.

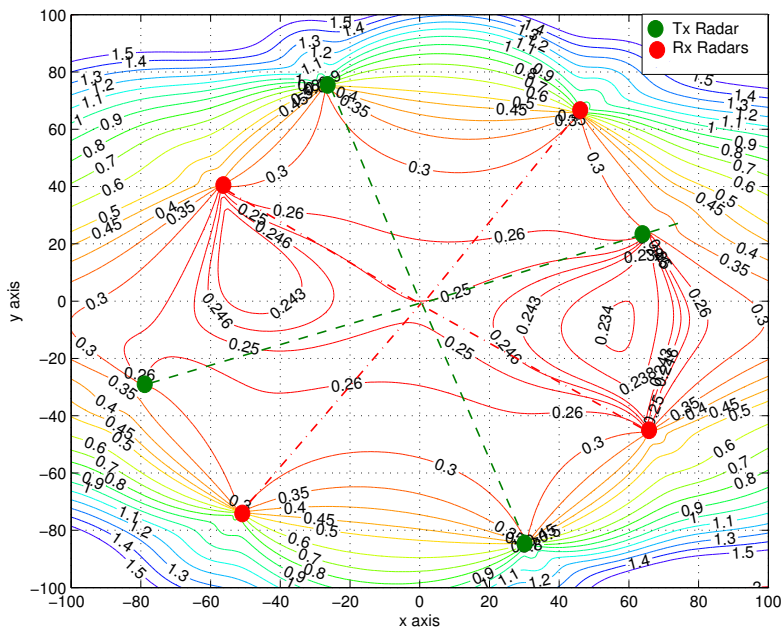


Figure 4: Coherent HyDOP contours with $M=N=4$.

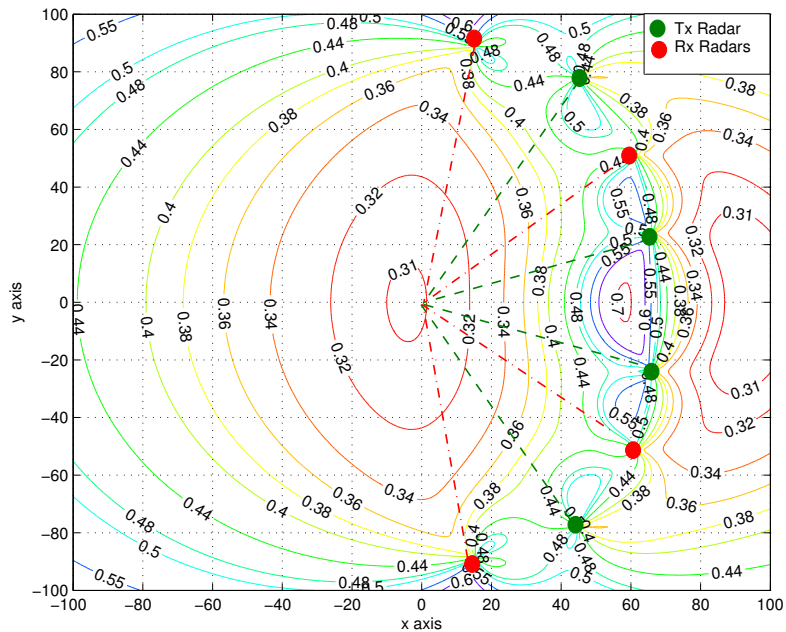


Figure 5: Non-coherent GDOP contours with $M=N=4$ - asymmetrical placement of radars.

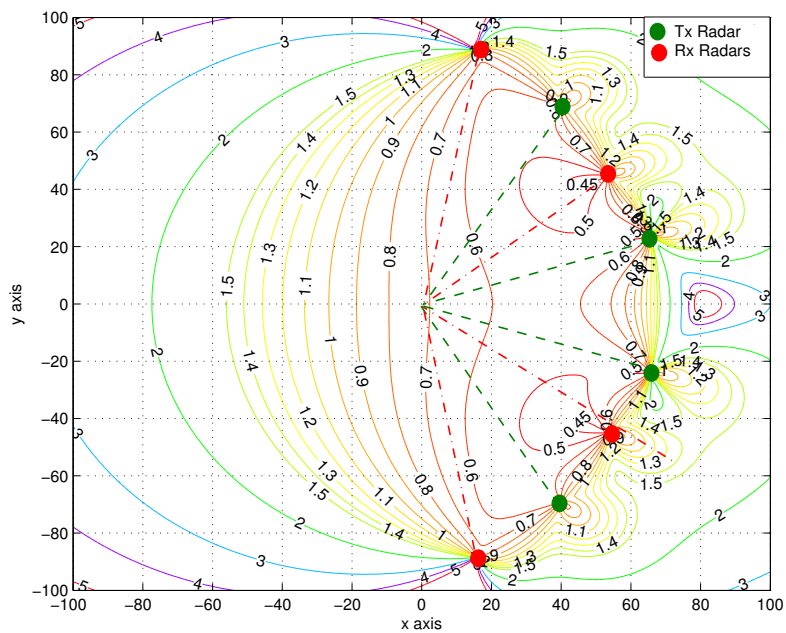


Figure 6: Coherent GDOP contours with $M=N=4$ - asymmetrical placement of radars.